International Journal of Mechanical Sciences 106 (2016) 184–193

Contents lists available at ScienceDirect

International Journal of Mechanical Sciences

journal homepage: www.elsevier.com/locate/ijmecsci

Asymptotic analysis of cold sandwich rolling

C.J. Cawthorn *, J.J. Minton, E.J. Brambley

Department of Applied Mathematics and Theoretical Physics, University of Cambridge, Centre for Mathematical Sciences, Cambridge CB3 0WA, UK

ARTICLE INFO

Article history:
Received 16 June 2015
Received in revised form
9 November 2015
Accepted 15 December 2015
Available online 22 December 2015

Keywords:
Metal rolling
Sandwich rolling
Metal forming
Asymptotic analysis

ABSTRACT

An analytical model for the cold rolling of sandwich sheets is proposed, assuming a rigid-plastic flow rule and Coulomb friction. Asymptotic analysis is used to solve the equations based on the assumptions of small aspect ratio and friction coefficient. This model relaxes the assumption, crucial to slab methods, that the stresses are uniformly distributed through the thickness of each material layer. Thus, our model is able to predict the through-thickness velocity and stress distributions. The leading-order behaviour is shown to be consistent with the slab method, and the predictions are compared with finite element simulations. Computation times are orders of magnitude smaller than finite element calculations.

1. Introduction

In the rolling of sheet metal, it is often desirable to sandwich a sheet of hard material between two sheets of softer metal. This can result in benefits such as improved thermal or electrical conductivity, anti-corrosion or frictional properties. In addition, sandwich sheet rolling is often an effective means of reducing the roll force required to thin high strength metals, leading to more efficient rolling processes [1].

Although sandwich sheet rolling has been the subject of several experimental studies [2–5], analytical studies to date have relied either on the classical upper bound (streamfunction) method [6] or slab theory [1,7]. Among these methods, slab theory produces the most accurate description of the stresses within the roll gap. However, even the most sophisticated slab model [7] assumes that the stress is vertically homogeneous within each material layer. In order to fulfil modern ambitions to predict and control the microstructure of materials during forming processes, one requires a model capable of correctly capturing through-thickness variation of stress and strain. While finite element simulations can deliver the required level of detail, computations typically take from several minutes to hours. This is too slow to be of practical use in online process control.

Here, a model is described for sandwich sheet rolling that captures through-thickness variation of the stress fields while remaining quick to evaluate. The asymptotic approach used by other authors for rolling [8,9] and extrusion [10] is modified and extended to account for the sandwich configuration. All of these models depend upon the assumption that the deformation zone has small aspect ratio, but they differ in their scaling assumptions and treatment of friction. Domanti and McElwain [8] make an additional assumption that the reduction of the sheet thickness is small. Although this simplifies the resulting calculation, it severely limits the range of validity of their model. Another model [9] does not require this assumption, but it employs a relative slip friction model, rather than the generally accepted Coulomb friction law. The extrusion model [10] assumes nothing about the reduction and uses Coulomb friction with a small friction coefficient, which is appropriate to most industrial rolling processes. The same scaling assumptions and friction model are applied here to the sandwich rolling configuration.

The assumptions made here are consistent with a popular slab model [7], except that here the stresses are allowed to be inhomogeneous through the thickness of the sheet. It is worth pointing out that the slab model [7] assumes a small friction coefficient without explicitly stating it as one of its 7 assumptions. In particular, when determining Eq. (14) in [7] the author neglects the term $\mu \tan \theta_c$. This is only consistent with the retention of other terms in Eq. (14) if the friction coefficient is small. Because of the similarities between our assumptions and those used in [7], any differences between these models arise solely due to the relaxation of the assumption, crucial to slab theory, that the stresses are homogeneous through the thickness of the material.

After developing the asymptotic model in Section 2, its predictions are compared with those of a finite element calculation performed using the Abaqus software [11]. The Abaqus model is described in Section 3, and the results are presented in Section 4. Finally, the accuracy and significance of our results are discussed in Section 5.

* Corresponding author.
E-mail address: C.J.Cawthorn@damtp.cam.ac.uk (C.J. Cawthorn).

http://dx.doi.org/10.1016/j.ijmecsci.2015.12.012

2. Asymptotic model

A sandwich sheet of total initial thickness $2h_0$ passes through identical circular rolls as shown in Fig. 1. In Fig. 1, and in the following analysis, variables with the subscript m refer to the central matrix layer, which has initial thickness $2\alpha h_0$ and yield stress k_m. By contrast, the subscript c identifies variables that apply to the cladding layers. The cladding layers each have initial thickness $(1-\alpha)h_0$ and yield stress $k_c=\beta k_m$. Attention is restricted to the region in which the sheet is in contact with the rolls, referred to as the roll gap. The thickness of the matrix layer as it passes through the roll gap is denoted by $2h_m(x)$, and is determined as part of the solution.

The rolls are assumed to be rigid, and the rolled material is represented as a non-hardening rigid-plastic undergoing plane strain. However, the following method could equally well describe the effect of roll deformation, by incorporating any deformation of the rolls into the roll shape, $h(x)$. It is assumed that there is no slip between the cladding and matrix layers, and Coulomb friction is imposed with a constant friction coefficient between the rolls and the cladding. Finally, the method relies on the key assumption that the aspect ratio of the roll gap,

$$\delta=\frac{h_0}{L}=\sqrt{\frac{h_0^2}{2R\Delta h}}, \tag{1}$$

is small.

Neglecting inertia, a quasi-steady solution is sought for the plastic flow through the roll gap. The relevant equations to be solved are therefore those of the plane strain stress equilibrium, with the von Mises yield criterion and the associated Levy–Mises flow rule.

2.1. Scaling and dimensionless equations

Throughout this analysis, horizontal distance is nondimensionalised with the characteristic roll gap length, $L=\sqrt{2R\Delta h}$, and vertical distance is scaled with the typical sheet half-thickness, h_0. The velocity (u,v) scales with the roll velocity $(R\Omega, R\Omega\delta)$. The Cauchy stresses, σ_{xx} and σ_{yy}, and deviatoric stresses, S_{xx} and S_{yy}, are all scaled with the matrix yield stress, k_m. The shear stress, S_{xy}, is assumed to scale with $\hat{\mu}k_m$, consistent with Coulomb friction. To complete the nondimensionalisation of the problem, the plastic parameter, λ, is scaled with $R\Omega/k_mL$. The assumption that the friction coefficient is small can be expressed by writing $\hat{\mu}=\mu\delta$, where μ is a quantity of approximate unit magnitude.

Under these scalings, the dimensionless form of the stress equilibrium (2)–(3), flow rule (4)–(6), and incompressibility relation (7) are

$$\frac{\partial\sigma_{xx}}{\partial x}+\mu\frac{\partial S_{xy}}{\partial y}=0, \tag{2}$$

$$\frac{\partial\sigma_{yy}}{\partial y}+\mu\delta^2\frac{\partial S_{xy}}{\partial x}=0, \tag{3}$$

$$\frac{\partial u}{\partial x}=\lambda S_{xx}, \tag{4}$$

$$\frac{\partial v}{\partial y}=\lambda S_{yy}, \tag{5}$$

$$\frac{\partial u}{\partial y}+\delta^2\frac{\partial v}{\partial x}=2\mu\delta^2\lambda S_{xy}, \tag{6}$$

$$\frac{\partial u}{\partial x}+\frac{\partial v}{\partial y}=0. \tag{7}$$

These equations all hold in both the cladding and matrix layers. By contrast, the yield criterion varies according to the yield stress in each layer:

$$S_{xx}^2+S_{yy}^2+2\mu^2\delta^2S_{xy}^2=\begin{cases}2 & \text{for } 0<y<h_m(x),\\ 2\beta^2 & \text{for } h_m(x)<y<h(x).\end{cases} \tag{8}$$

Symmetry in the horizontal axis requires the boundary conditions

$$v(x,0)=0 \quad \text{and} \quad S_{xy}(x,0)=0, \tag{9}$$

while the absence of flow normal to the roll surface gives

$$v(x,h(x))=h'(x)u(x,h(x)). \tag{10}$$

The roll shape, described by $h(x)$, will typically be circular. However, no assumptions are made about the roll profile, other than that it varies gradually over a lengthscale comparable to L.

The Coulomb friction condition to be applied on the roll surface may be expressed as

$$\mu\left(1-\delta^2h'^2\right)S_{xy}+(S_{yy}-S_{xx})h'=\mp\mu\left[\sigma_{yy}+\delta^2\left(h'^2\sigma_{xx}-2\mu h'S_{xy}\right)\right], \tag{11}$$

with all terms evaluated at $y=h(x)$. The $\mp$ sign in (11) is chosen according to the slip velocity of the sheet over the rolls.

There exists a position, x_N, referred to as the neutral point, where the speed of the sheet surface relative to the roller is zero. Throughout this analysis, the convention is adopted that the upper signs refer to the entrance region, $x<x_N$, where the rolls drag the slower-moving material into the roll gap. The lower signs refer to the exit region, $x>x_N$, in which the sheet moves faster than the rolls, so friction opposes the escape of the sheet from the gap. At

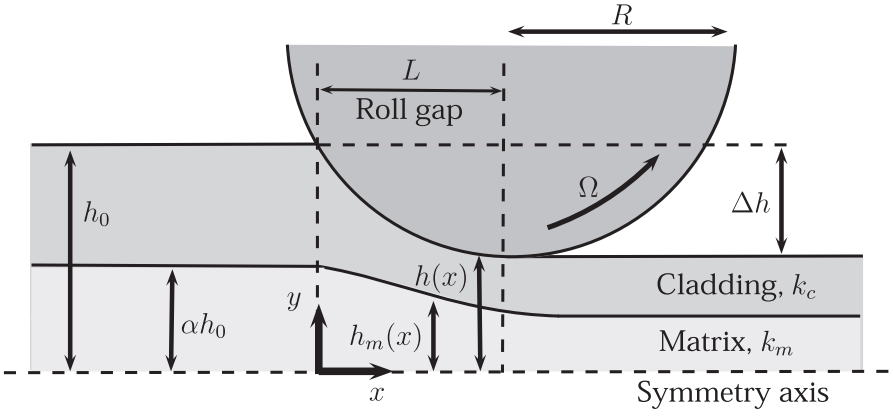

Fig. 1. Diagram of sandwich sheet rolling. Only one roller and half of the sandwich sheet are shown; the configuration is symmetric with the x-axis (lower dashed line) as the symmetry axis.

the neutral point, Coulomb friction gives rise to a sharp jump in shear stress, which in turn creates discontinuities in the stress and velocity components in this model. This is an undesirable but unavoidable consequence of using Coulomb friction without some form of smoothing.

The model assumes no slip between the cladding and matrix material, so that

$$u_c = u_m \quad \text{and} \quad v_c = v_m \quad \text{on } y = h_m(x). \tag{12}$$

The shape of the interface, $h_m(x)$, is determined by the no-flux constraint

$$v_m = h_m' u_m \quad \text{on } y = h_m(x). \tag{13}$$

Furthermore, the normal and shear stresses are continuous across the interface, thus

$$\left[\sigma_{yy} - \delta^2\left(2\mu h_m' S_{xy} - h_m'^2 \sigma_{xx}\right)\right]_m^c = 0, \tag{14}$$

and

$$\left[\mu\left(1-\delta^2 h_m'^2\right)S_{xy} - h_m'(S_{xx} - S_{yy})\right]_m^c = 0, \tag{15}$$

on $y = h_m(x)$. These interfacial stresses are important measures of the adhesion needed to maintain the bonding between the two materials that is assumed by our model.

Assuming that (dimensional) tensions per unit width $\hat{T}_{in}$ and $\hat{T}_{out}$ are applied at the entrance and exit respectively, the horizontal stress must satisfy the conditions

$$\frac{\hat{T}_{in}}{h_0 k_m} = \int_0^{h_m(0)} \sigma_{xxm}(0,y)\,\mathrm{d}y + \int_{h_m(0)}^{1} \sigma_{xxc}(0,y)\,\mathrm{d}y, \tag{16}$$

$$\frac{\hat{T}_{out}}{h_0 k_m} = \int_0^{h_m(1)} \sigma_{xxm}(1,y)\,\mathrm{d}y + \int_{h_m(1)}^{1-r} \sigma_{xxc}(1,y)\,\mathrm{d}y. \tag{17}$$

In order to solve Eqs. (2)–(17) the stress components, velocity components, and plastic parameter are expanded as asymptotic series in the small parameter δ,

$$A(x,y) = A^{(0)}(x,y) + \delta^2 A^{(2)}(x,y) + O\left(\delta^4\right), \tag{18}$$

where A represents any of the expanded variables. The a priori unknown location of the interface between the matrix and cladding is similarly expanded:

$$h_m(x) = h_m^{(0)}(x) + \delta^2 h_m^{(2)}(x) + O\left(\delta^4\right). \tag{19}$$

Terms proportional to δ are omitted here because δ only ever appears as δ^2 in Eqs. (2)–(17).

2.2. Leading-order solution

The leading-order solution is determined by considering only those terms independent of δ in Eqs. (2)–(17). Recognising from (6) that $u^{(0)}$ is independent of y in each layer, applying the no-slip condition (12) at the interface between the layers leads to $u_m^{(0)} = u_c^{(0)} = u_0(x)$. Volume conservation then requires that

$$u_0(x) = \frac{h_N}{h(x)}. \tag{20}$$

In (20), $h_N = h(x_N)$ is defined to be the roll gap semi-thickness at the neutral point, where the choice of our scaling requires that $u_c^{(0)}(x_N) = 1$. Integrating (7),

$$v_m^{(0)} = v_c^{(0)} = \frac{y h_N h'}{h^2}. \tag{21}$$

Applying conservation of volume to the matrix material requires that $h_m^{(0)}(x) = \alpha h(x)$.

To determine the stresses, it is observed from (4), (5) and (7) that $S_{xx}^{(0)} = -S_{yy}^{(0)}$ in each layer, and then the yield criterion (8) gives

$$S_{xxm}^{(0)} = -S_{yym}^{(0)} = 1 \quad \text{and} \quad S_{xxc}^{(0)} = -S_{yyc}^{(0)} = \beta. \tag{22}$$

The quadratic yield criterion (8) leaves some ambiguity as to the sign of the deviatoric stresses. The signs chosen in (22) correspond to plastic loading ($\lambda > 0$).

At leading order, (3) implies that the leading-order vertical stress, $\sigma_{yy}^{(0)}$, is also independent of y in each layer, and continuity of vertical stress (14) implies that $\sigma_{yym}^{(0)} = \sigma_{yyc}^{(0)} = \sigma_0(x)$. Noting further that the definition of deviatoric stress gives

$$\sigma_{xx} = \sigma_{yy} + S_{xx} - S_{yy}, \tag{23}$$

substituting (23) for $\sigma_{xx}^{(0)}$ in (2) and integrating in y over each region leads to the differential equation obeyed by σ_0,

$$\alpha h \frac{\mathrm{d}\sigma_0}{\mathrm{d}x} + \mu S_{xym}^{(0)}\Big|_{y=\alpha h} = 0, \tag{24}$$

$$(1-\alpha)h\frac{\mathrm{d}\sigma_0}{\mathrm{d}x} + \mu S_{xyc}^{(0)}\Big|_{y=h} - \mu S_{xyc}^{(0)}\Big|_{y=\alpha h} = 0. \tag{25}$$

Eliminating the change in shear stress along $h_m^{(0)}(x) = \alpha h$ using (15) and the roll shear stress using (11), and then summing (24) and (25) produces the key leading-order result

$$h\frac{\mathrm{d}\sigma_0}{\mathrm{d}x} \mp \mu\sigma_0 = 2(\alpha\beta - \alpha - \beta)h'. \tag{26}$$

The leading-order form of the lateral boundary conditions (16) and (17) provides the boundary conditions for this differential equation

$$\frac{\hat{T}_{in}}{h_0 k_m} = \sigma_0(0) + 2\left[\beta(1-\alpha)+\alpha\right], \tag{27}$$

$$\frac{\hat{T}_{out}}{(h_0 - \Delta h)k_m} = \sigma_0(1) + 2\left[\beta(1-\alpha)+\alpha\right]. \tag{28}$$

For a general roll gap profile, $\sigma_0(x)$ is found by integrating (26) separately from the entrance and exit, using the boundary conditions (27) and (28) respectively. By continuity of the longitudinal stress, the neutral point, x_N, must be the point at which these two solutions coincide.

Having obtained $\sigma_0(x)$ by solving (26) numerically or otherwise, one can integrate (2) to determine the shear stress, using the relation (15) to connect the solutions at $y = h_m^{(0)}(x)$,

$$S_{xym}^{(0)} = -\frac{y\sigma_0'}{\mu}, \tag{29}$$

$$S_{xyc}^{(0)} = -\frac{1}{\mu}\left[y\sigma_0' - 2(\beta-1)\alpha h'\right]. \tag{30}$$

Finally, the plastic parameter in each material can be determined using (4)

$$\lambda_m^{(0)} = -\frac{h_N h'}{h^2}, \tag{31}$$

$$\lambda_c^{(0)} = -\frac{h_N h'}{\beta h^2}. \tag{32}$$

2.3. $O\left(\delta^2\right)$ correction

Having determined the leading-order solution, this section proceeds to develop the correction resulting from the terms of order δ^2 in Eqs. (2)–(17). The second-order equations are

$$\frac{\partial \sigma_{xx}^{(2)}}{\partial x} + \mu\frac{\partial S_{xy}^{(2)}}{\partial y} = 0, \tag{33}$$

$$\frac{\partial \sigma_{yy}^{(2)}}{\partial y}+\mu\frac{\partial S_{xy}^{(0)}}{\partial x}=0, \tag{34}$$

$$\frac{\partial u^{(2)}}{\partial x}=\lambda^{(2)}S_{xx}^{(0)}+\lambda^{(0)}S_{xx}^{(2)}, \tag{35}$$

$$\frac{\partial v^{(2)}}{\partial y}=\lambda^{(2)}S_{yy}^{(0)}+\lambda^{(0)}S_{yy}^{(2)}, \tag{36}$$

$$\frac{\partial u^{(2)}}{\partial y}+\frac{\partial v^{(0)}}{\partial x}=2\mu\lambda^{(0)}S_{xy}^{(0)}, \tag{37}$$

$$\frac{\partial u^{(2)}}{\partial x}+\frac{\partial v^{(2)}}{\partial y}=0, \tag{38}$$

$$S_{xx}^{(0)}S_{xx}^{(2)}+S_{yy}^{(0)}S_{yy}^{(2)}+\mu^2S_{xy}^{(0)2}=0. \tag{39}$$

From Eqs. (34) and (37), it is clear that $\sigma_{xy}^{(2)}$ and $u^{(2)}$ are not independent of y, unlike $\sigma_{yy}^{(0)}$ and $u^{(0)}$. In each case, the y-dependence is determined by the leading-order solution.

Integrating (37) in each layer and applying the no-slip relation (12) leads to

$$u_m^{(2)}=u_2(x)+\frac{h_N}{2h^3}\left(2h'^2-hh''+2hh'\sigma_0'\right)y^2, \tag{40}$$

and

$$u_c^{(2)}=u_2(x)+\frac{h_N}{2h^3}\left(2h'^2-hh''+\frac{2hh'\sigma_0'}{\beta}\right)y^2-4\alpha\left(\frac{\beta-1}{\beta}\right)\frac{h_Nh'^2}{h^2}(y-\alpha h)+\alpha^2\left(\frac{\beta-1}{\beta}\right)h_Nh'\sigma_0'. \tag{41}$$

The function $u_2(x)$ is determined by noting that the correction to volume flux through any vertical surface must be zero,

$$\int_0^{h(x)}u^{(2)}\,\mathrm{d}y=0 \quad \text{for all } x. \tag{42}$$

Thus,

$$u_2(x)=\frac{h_N}{6h}\left(hh''-2h'^2-\frac{2hh'\sigma_0'}{\beta}\right)+\frac{\alpha h_N}{3h}\left(\frac{\beta-1}{\beta}\right)\left[6(\alpha-1)^2h'^2+(2\alpha-3)\alpha hh'\sigma_0'\right]. \tag{43}$$

Having determined the correction to u, the correction to v in each layer can be determined by integrating (38), again applying the no-slip condition (12) to the velocity field at $y=h_m^{(0)}=\alpha h$ to obtain

$$v_m^{(2)}=-yu_2+\frac{h_Ny^3}{6h^4}\left[6h'^3+h^2h'''-6hh'h''+4hh'^2\sigma_0'-2h^2(h''\sigma_0'+h'\sigma_0'')\right], \tag{44}$$

$$\begin{aligned}v_c^{(2)}=&-yu_2'+\frac{1}{3}\alpha^3h_N\left(\frac{\beta-1}{\beta}\right)\left[2h'^2\sigma_0'-hh''\sigma_0'-hh'\sigma_0''\right]\\&-\frac{\alpha^2h_N}{h^2}\left(\frac{\beta-1}{\beta}\right)\left[4h'^3+h^2h''\sigma_0'+h^2h'\sigma_0''\right](y-\alpha h)\\&+\frac{4\alpha h_N}{h^3}\left(\frac{\beta-1}{\beta}\right)[hh'h''-h'^3](y-\alpha h)^2+\frac{h_Ny^3}{6h^4}\Big(6h'^3+h^2h'''\\&-6hh'h''+\tfrac{4}{\beta}hh'^2\sigma_0'-\tfrac{2}{\beta}h^2(h''\sigma_0'+h'\sigma_0'')\Big),\end{aligned} \tag{45}$$

where $u_2'(x)$ can be obtained by differentiating (43). Furthermore, the condition that there is no flux of material across the interface between the two layers (13), expanded about the leading-order interface, $h_m=\alpha h$, requires that

$$v_m^{(2)}+\frac{\partial v_m^{(0)}}{\partial y}h_m^{(2)}=\alpha h'\left(u_m^{(2)}+\frac{\partial u_m^{(0)}}{\partial y}h_m^{(2)}\right)+\mathrm{d}h_m^{(2)}\mathrm{d}xu_m^{(0)}, \tag{46}$$

at $y=\alpha h(x)$. Substituting for the known velocities and integrating leads to

$$h_m^{(2)}=\frac{h}{h_N}\int_0^x v_m^{(2)}\left[t,\alpha h(t)\right]-\alpha h'(t)u_m^{(2)}\left[t,\alpha h(t)\right]\,\mathrm{d}t. \tag{47}$$

As was the case at leading order, the plane strain assumption together with incompressibility requires that $S_{xx}^{(2)}=-S_{yy}^{(2)}$. The yield condition (39) then gives

$$S_{xxm}^{(2)}=-\frac{1}{2}\sigma_0'^2y^2, \tag{48}$$

$$S_{xxc}^{(2)}=-\frac{1}{2\beta}\sigma_0'^2y^2+2\alpha\left(\frac{\beta-1}{\beta}\right)\left[h'\sigma_0'y-(\beta-1)\alpha h'^2\right]. \tag{49}$$

Integrating (34) and using the continuity of normal stress (14) gives the y-dependence of $\sigma_{yy}^{(2)}$ in each layer:

$$\sigma_{yym}^{(2)}=\sigma_2(x)+\frac{1}{2}\sigma_0''y^2, \tag{50}$$

$$\sigma_{yyc}^{(2)}=\sigma_2(x)+\frac{1}{2}\sigma_0''y^2-2\alpha(\beta-1)\left[h''y-\alpha(hh''+h'^2)\right]. \tag{51}$$

The ordinary differential equation for $\sigma_2(x)$ is found by computing the associated longitudinal stresses using (23), integrating (33) within each layer, and summing the result in the same way as leading to (26), giving

$$\begin{aligned}h\frac{\mathrm{d}\sigma_2}{\mathrm{d}x}=&-\frac{1}{6}h^3\left(\sigma_0'''-\frac{4}{\beta}\sigma_0'\sigma_0''\right)-\mu\left(S_{xyc}^{(2)}\Big|_{y=h}-S_{xyc}^{(2)}\Big|_{y=\alpha h}+S_{xym}^{(2)}\Big|_{y=\alpha h}\right)\\&+\frac{2}{3}\left(\frac{\beta-1}{\beta}\right)\alpha^3h^3\sigma_0'\sigma_0''+\alpha(1-\alpha)^2(\beta-1)h^2h'''\\&-2\alpha(1-\alpha^2)\left(\frac{\beta-1}{\beta}\right)h^2(h''\sigma_0'+h'\sigma_0'')\\&-2\alpha^2(1-\alpha)\left(\frac{\beta-1}{\beta}\right)(4-\beta)hh'h''.\end{aligned} \tag{52}$$

The shear stresses are obtained by evaluating the boundary conditions (11) and (15) to $O\left(\delta^2\right)$

$$\mu(S_{xyc}^{(2)}-S_{xym}^{(2)})\Big|_{y=\alpha h}=2(\beta-1)h_m^{(2)'}+\alpha^3\left(\frac{\beta-1}{\beta}\right)\left[4hh'^2\sigma_0'+h^2h'\sigma_0'^2-2(\beta-2)h'^3\right] \tag{53}$$

$$\begin{aligned}\mu S_{xyc}^{(2)}\Big|_{y=h}=&\mp\left[\sigma_2+\frac{1}{2}h^2\sigma_0'+(2\beta+\sigma_0)h'^2\right]-(h'\pm2\mu)hh'\sigma_0'\\&-\frac{1}{\beta}h^2h'\sigma_0'^2+4\alpha\left(\frac{\beta-1}{\beta}\right)hh'^2\sigma_0'+2\alpha(\beta-1)\Big[(1\\&-2\alpha\left(\frac{\beta-1}{\beta}\right)\Big)h'^3\mp\mu(\alpha-2)h'^2\mp\mu(\alpha-1)hh''\Big]\end{aligned} \tag{54}$$

Substituting these into (52), the differential equation for σ_2 becomes

$$h\frac{\mathrm{d}\sigma_2}{\mathrm{d}x}\mp\mu\sigma_2=\mathcal{F}(x). \tag{55}$$

The inhomogeneous term in (55) is given by

$$\begin{aligned}\mathcal{F}(x)=&-\frac{1}{6}h^3\sigma_0'''+\frac{1}{\beta}h^2h'\sigma_0'^2+\frac{2}{3\beta}h^3\sigma_0'\sigma_0''+(h'\pm2\mu)hh'\sigma_0'\pm\frac{1}{2}\mu\sigma_0''h^2\\&\pm\mu h'^2(\sigma_0+2\beta)+2(\beta-1)h_m^{(2)'}+\alpha^3\left(\frac{\beta-1}{\beta}\right)\Big[4hh'^2\sigma_0'+h^2h'\sigma_0'^2\\&-2(\beta-2)h'^3+\frac{2}{3}h^3\sigma_0'\sigma_0''\Big]-2\alpha(\beta-1)\Big[\Big(1-2\alpha\left(\frac{\beta-1}{\beta}\right)\Big)h'^3\\&\mp\mu(\alpha-2)h'^2\mp\mu(\alpha-1)hh''\Big]-4\alpha\left(\frac{\beta-1}{\beta}\right)hh'^2\sigma_0'\\&-2\alpha(1-\alpha^2)\left(\frac{\beta-1}{\beta}\right)h^2\left[h''\sigma_0'+h'\sigma_0''\right]\end{aligned}$$

$$+\alpha(1-\alpha)\left(\frac{\beta-1}{\beta}\right)\left[(1-\alpha)\beta h^2 h''' - 2\alpha(4-\beta)hh'h''\right]. \quad (56)$$

As before, the upper signs refer to the entrance region, $x < x_N$; in which the rolls move more quickly than the sheet; whereas the lower signs refer to the exit, $x > x_N$. The boundary conditions are set at each end of the roll gap by considering that

$$\int_0^h \sigma_{xx}^{(2)}\,\mathrm{d}y = 0 \quad \text{at } x = 0, 1; \quad (57)$$

where $\sigma_{xx}^{(2)} = \sigma_{yy}^{(2)} + S_{xx}^{(2)} - S_{yy}^{(2)}$ in both the cladding and the matrix material.

The correction to shear stress can be computed by integrating (33)

$$S_{xym}^{(2)} = -\frac{1}{\mu}\int_0^y \frac{\partial \sigma_{xxm}^{(2)}}{x}\,\mathrm{d}y', \quad (58)$$

$$S_{xyc}^{(2)} = S_{xyc}^{(2)}\Big|_{y=\alpha h} - S_{xym}^{(2)}\Big|_{y=\alpha h} - \frac{1}{\mu}\int_{\alpha h}^y \frac{\partial \sigma_{xxc}^{(2)}}{x}\,\mathrm{d}y'. \quad (59)$$

Eq. (53) is used again to evaluate the jump in $S_{xy}^{(2)}$ at the bonded interface.

Finally, the correction to the plastic parameter can be found using (35)

$$\lambda^{(2)} = \frac{1}{S_{xx}^{(0)}}\left(\frac{\partial u^{(2)}}{x} - \lambda^{(0)} S_{xx}^{(2)}\right). \quad (60)$$

This asymptotic expansion could be continued to higher orders, the next of which will be at $O(\delta^4)$. However, note that all of Eqs. (2)–(17) involve terms of order at most δ^2. This means that the inclusion of higher order corrections is unlikely to introduce any new qualitative behaviour to the results. Moreover, for rolling of thin sheets ($\delta \approx 0.1$) the magnitude of the higher order corrections is likely to be small enough to be of little practical significance. The asymptotic analysis is therefore concluded here.

To summarise the solution procedure, it is necessary to first integrate the leading-order stress Eq. (26) from $x=0$ and $x=1$ subject to the boundary conditions (16) and (17), in order to find $\sigma_0(x)$ for a specified gap profile, $h(x)$. One must then evaluate the forcing term given by (56) before integrating (55) to find the second-order function $\sigma_2(x)$. All of the leading- and second-order velocity and stress components may be calculated in terms of these functions using the remaining results in this section. MATLAB code to perform this calculation is provided in the supplementary material.

2.4. Relation to previous works

As mentioned in the Introduction, the assumptions of the present model differ from previous works. Nevertheless, there are some important similarities that should be highlighted.

Firstly, note that Tzou [7] obtains an equation equivalent to the leading-order stress equation (26) via slab theory, and goes on to obtain an approximate solution for a parabolic roll gap profile. The predictions of the slab theory model from [7] are therefore identical to the leading-order solution described in Section 2.2. This is not surprising, because the assumption of small aspect ratio precludes the possibility of through-thickness variations in stress in the leading-order asymptotic model. For the remainder of this paper, the leading-order asymptotic solution will be referred to as 'the slab model', with the understanding that the results of both are equivalent.

The second-order correction described in Section 2.3 introduces through-thickness variation in all quantities. It is therefore fundamentally different from the slab theory solution. Although no other authors have reported such results for sandwich rolling, comparisons can be drawn with other results in the case of a homogeneous sheet ($\beta = 1$). Although no comparable result exists combining the present scaling with Coulomb friction in the rolling literature, a model for extrusion [10] does use this combination. Because an extrusion die is typically held stationary, there is no analogue of the entrance region observed in rolling. However, the present results agree exactly with the extrusion model [10] for the exiting flow in the case of a homogeneous sheet. The relaxation of assumptions regarding the size of the reduction here also means that this result is more flexible than that of Domanti and McElwain [8].

Note also that the $O(\delta^2)$ correction described in Section 2.3 should include a correction to the neutral point position, x_N. Although one might hope to obtain this correction by finding the location at which the tangential sheet speed matches that of the rolls, the discontinuity in $u_c^{(2)}$, which arises from the jump in $S_{xy}^{(0)}$, means that no unique solution for x_N exists. In truth, the dynamics in the vicinity of the neutral point are more complicated than can be explained by the current model. It is typically asserted (see [8], for example) that material will stick to a small section of the roll near the neutral point, allowing the shear stress to change smoothly from one direction to the other. It is thought that this, in turn, causes a sub-yield elastic plug to form.

While some authors avoid this problem by smoothing the friction discontinuity (either deliberately, see [12], or through numerical under-resolution) or by using a relative slip model when the velocity of the sheet relative to the roller is small [9], the correct approach may be to perform an inner asymptotic expansion of the small region over which the shear stress changes sign, and match this to the outer solution. However, the conjectured presence of a sub-yield region suggests that elasticity is very important to the dynamics in this region, and to include this would step outside the scope of this model. For now, it is noted that the presence of the mild discontinuity near the neutral point is an artefact of rigidly enforcing the Coulomb friction model, and is an approximation to a rapid but smooth change in reality. In practice this is not worrying; Section 4.4 demonstrates that reasonable predictions can still be made for the rest of the roll gap.

3. Finite element simulation

In the absence of detailed experimental results, the predictions of the asymptotic model are compared with finite element simulations using the Abaqus package. All of the simulations used a mild modification of the plane strain rolling configuration described in Section 1.3.11 of [11], with the sections defining the matrix and cladding material joined using simple 'pin' constraints along the bonded interface. Rolling was initiated by giving an initially undeformed sheet an initial velocity of magnitude $R\Omega$ toward the rolls, which were forced to rotate at a constant rate. The yield stress of the matrix material was fixed at 300 MPa, while the yield stress of the cladding was allowed to vary to achieve a range of values for β. Unlike the analytical model in Section 2, Abaqus requires a degree of elasticity in material behaviour. Each material was given Young's modulus, E, 500 times larger than its plastic yield stress, and Poisson ratio, ν, equal to 0.35. This is fairly typical of steel or aluminium alloys. Sensitivity to the exact choice of elastic parameters will be discussed in Section 4.1. A brief mesh sensitivity study confirmed that the choice of mesh did not strongly affect the results.

4. Results

In this section, several findings are presented based on the comparison of the model described in Section 2 with the simulations described in Section 3. As mentioned in Section 2.4, the term

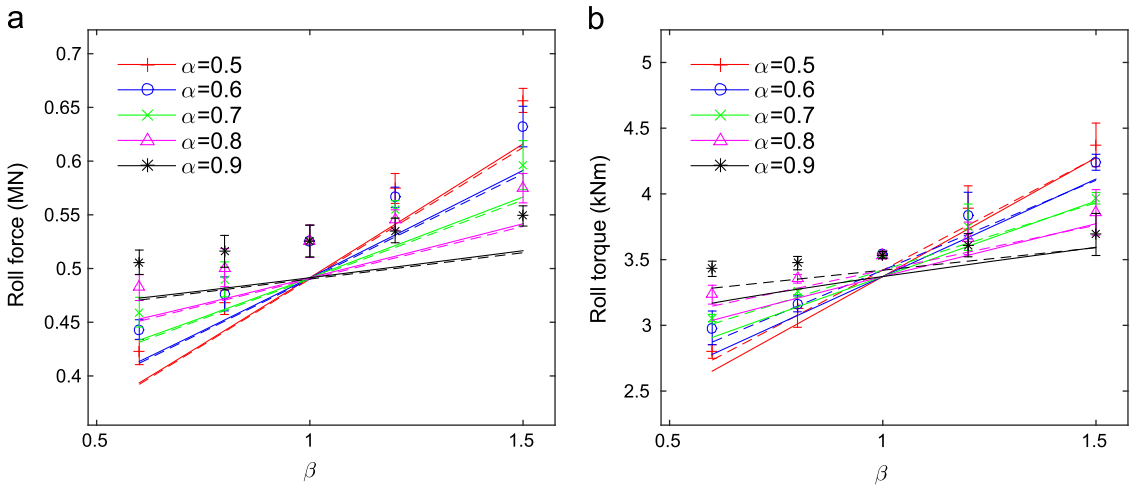

Fig. 2. Variation of (a) force and (b) torque with yield strength ratio, β, for a range of sheet thickness ratio, α. Solid lines show results from the asymptotic model, dashed lines show the slab model results, and symbols show finite element results. The error bars indicate the spread of results under variation of Young's modulus ($E=100k$, $500k$, $1000k$) and Poisson ratio ($\nu=0.3, 0.35, 0.4$).

'slab model' is used to refer interchangably to both the leading-order asymptotic solution and the actual slab model of Tzou [7].

When investigating the effect of varying the process parameters, it is useful to define a basic case. For the purpose of this section, we define the basic case by the dimensionless parameters $(\alpha, \beta, \delta, r, \hat{\mu}) = (0.7, 0.8, 0.35, 0.2, 0.1)$. This corresponds to a 10 mm thick sheet being reduced to 8 mm thickness by rolls of radius 100 mm, which is fairly typical of industrial rolling.

4.1. Similarity to slab theory

Since roll force and torque are the two most important control parameters in rolling, roll force and torque predictions are used here as a means of comparison between the slab model, asymptotic model, and the finite element simulations. Predictions and simulated results for a range of α and β are shown in Fig. 2.

The most striking feature of the results is that the analytical models consistently under-predict the forces by up to 10%. The predicted torques are in much better agreement with the simulations, but still tend to be underestimates. The reason for the discrepancy in forces is likely to involve the elastic effects introduced in the Abaqus simulation. This will be discussed in more detail in Section 4.4. Nevertheless, the variation of force and torque in response to changes in sandwich composition relative to the homogeneous case ($\beta=1$) is well captured qualitatively and quantitatively by both the slab model and corrected asymptotic results. The intuitive expectation that a thicker and/or softer cladding will result in smaller rolling forces and torques is met by the results shown. The error bars in Fig. 2 show the effect of varying the elastic parameters that are not accounted for by the asymptotic model. For a range of elastic behaviours consistent with most steels and aluminium alloys, the results are rather insensitive to the precise elastic parameters chosen.

It is interesting to note that the two analytical models are in close agreement for most parameter values. If one were to be interested only in predicting the force and torque necessary to roll the sandwich sheet, one would therefore gain little by including the asymptotic correction. The $O(\delta^2)$ correction offers a small improvement in force predictions at the cost of a small reduction in accuracy for torques. However, as noted earlier, the real advantage of the $O(\delta^2)$ correction lies in predicting through-thickness variation, as described in Section 4.3.

4.2. Range of validity

In order to establish the practical range of validity of the asymptotic model, other parameters are now varied. Fig. 3 illustrates the effect of varying δ, via the roller radius, R, for a fixed sheet composition, $(\alpha, \beta) = (0.7, 0.8)$. Although the agreement is good for most of the values of R chosen, the relative error in force is particularly small (less than 4%) for $0.08\ \text{m} < R < 0.15\ \text{m}$, which corresponds to $0.29 < \delta < 0.40$. This range contains most values of δ appropriate to industrial rolling processes.

Fig. 4 illustrates the accuracy of the model under variation of the friction coefficient, $\hat{\mu}$. The predictions are seen to be reasonably accurate for values of $\hat{\mu}$ in the vicinity of 0.1, but fairly rapidly diverge away from the simulated results for $\hat{\mu} > 0.2$. For smaller friction coefficients, the simulated force and torques are more noisy, but seem to indicate a sharp decrease in the force and torque. Although the force behaviour is not captured by the asymptotic model, the decrease in torque is represented in the prediction. For small $\hat{\mu}$, the neutral point lies at the exit of the roll gap, so the entire roller surface acts to pull the sheet through the roll gap. At approximately $\hat{\mu} = 0.08$ the neutral point begins to move into the roll gap, introducing an opposing shear stress to the roller and stabilising the torque. Increasing $\hat{\mu}$ beyond 0.2 breaks the assumption of a small $\hat{\mu}$, so the equations ought to be rescaled to correctly predict the behaviour here. However, the asymptotic model performs well for the range of friction coefficients typically occurring in industry.

The sensitivity of the results to the reduction, $r = \Delta h/h_0$, was also investigated, and typical results are shown in Fig. 5. The asymptotic model predicts forces and torques reasonably accurately across almost all of the reductions studied. While the model continues to make predictions for larger reductions than those shown without issue, the simulations failed as a result of the velocity-based initiation of the process. Instead of being captured by the friction of the rolls, the sheet was found to bounce backwards, away from the rolls. As reductions of 20% or less are most typical of industrial rolling processes, larger reductions have not been investigated here in any more detail.

4.3. Prediction of through-thickness variation

Although Section 4.1 demonstrated that the slab and asymptotic models are in general agreement when predicting roll force and

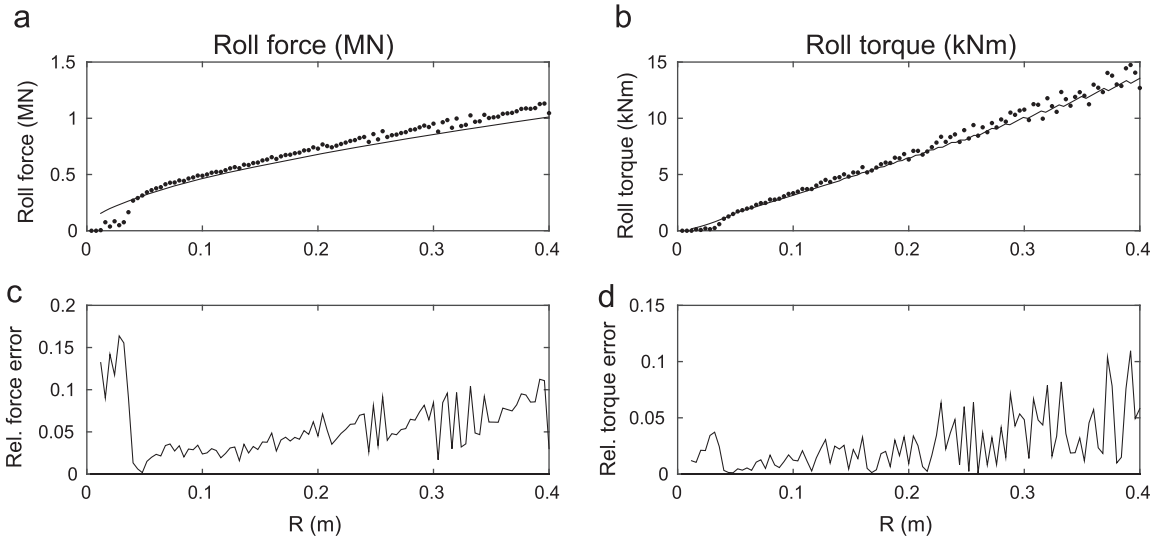

Fig. 3. Variation of force and torque with the roller radius R. Panels (a) and (b) compare the force and torque predictions (lines) with simulation results (symbols), while panels (c) and (d) show the relative errors in force and torque respectively.

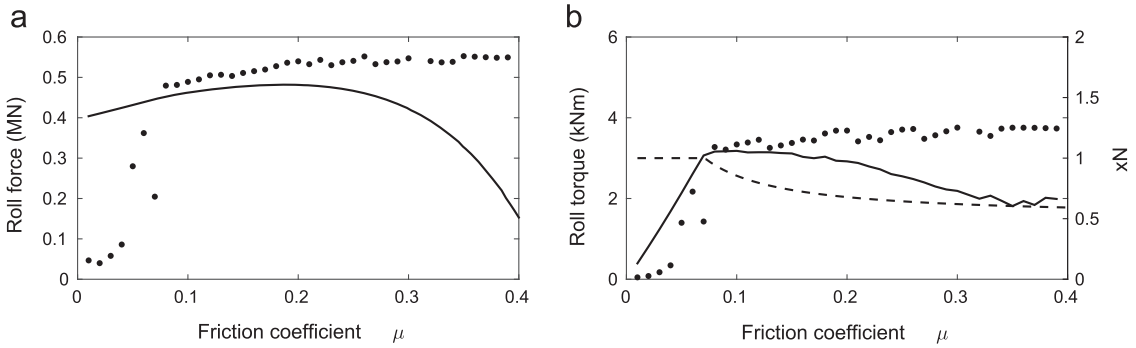

Fig. 4. Variation of (a) force and (b) torque with the friction coefficient, μ. In each plot, simulation results (symbols) are compared with the model predictions (solid lines). In panel (b), the neutral point position, x_N, is shown as a dashed line.

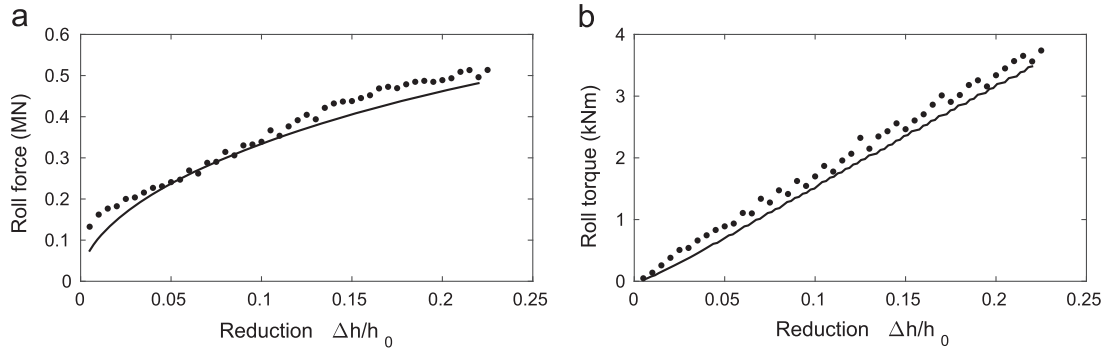

Fig. 5. Variation of (a) force and (b) torque with the reduction, $r = \Delta h/h_0$. In each plot, simulation results (symbols) are compared with the model predictions (solid lines).

torque, the internal stress structure differs substantially between the two models. The differences result from relaxing the assumption of stress uniformity through the thickness of each material.

For moderate values of the yield stress ratio, β, the manner in which the asymptotic results differ from the slab model predictions appears to be qualitatively similar for a wide range of parameters. Thus, the differences are illustrated by considering just the basic case described at the beginning of this section.

Figs. 6 and 7 show typical velocity and stress distributions for the basic case. In order to illustrate the effect of the asymptotic correction derived in Section 2.3, both the slab theory and asymptotically corrected solutions are plotted. In each case, the plots are generally quite similar. The horizontal velocity is largely uniform in y, but the correction adds a small degree of shear, consistent with the action of friction. Similarly, the stresses are dominated by the typical 'friction hill' near $x=0.85$, but there is a small local minimum (in magnitude) in the longitudinal stresses near $x=0.35$. This arises due to the competition between the frictional term ($\mp\mu\sigma_0$) and the geometric term (proportional to $-h'$) in the stress equation (26). The former term acts to pull material into the roll gap, while the latter resists compression by the rolls, leading to a small plateau where these effects are in

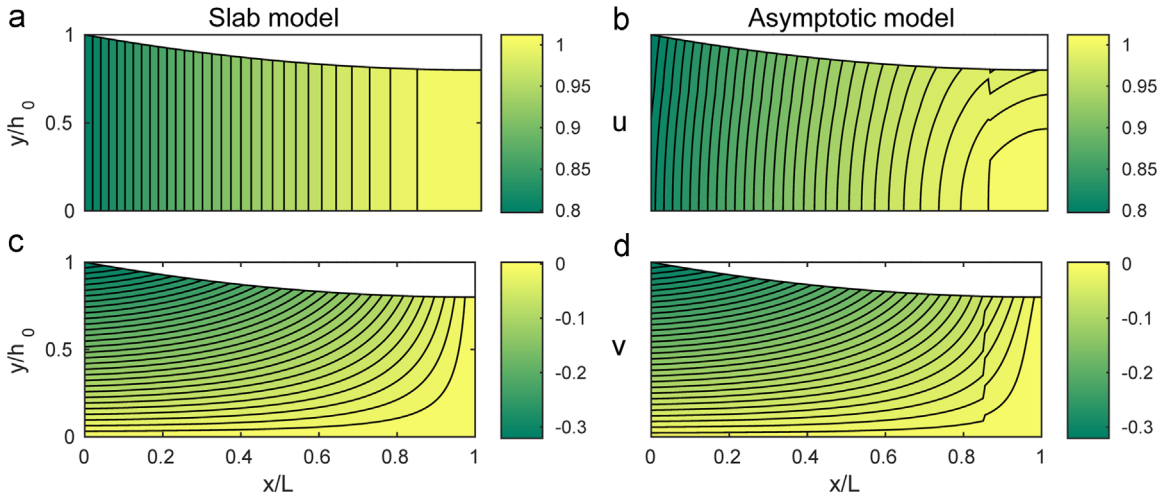

Fig. 6. Velocities in the roll gap for a moderate roller radius ($R = 0.1$ m, $\delta = 0.35$). The (a, b) horizontal and (c, d) vertical velocities are shown for the (a, c) slab model and (b, d) corrected asymptotic model.

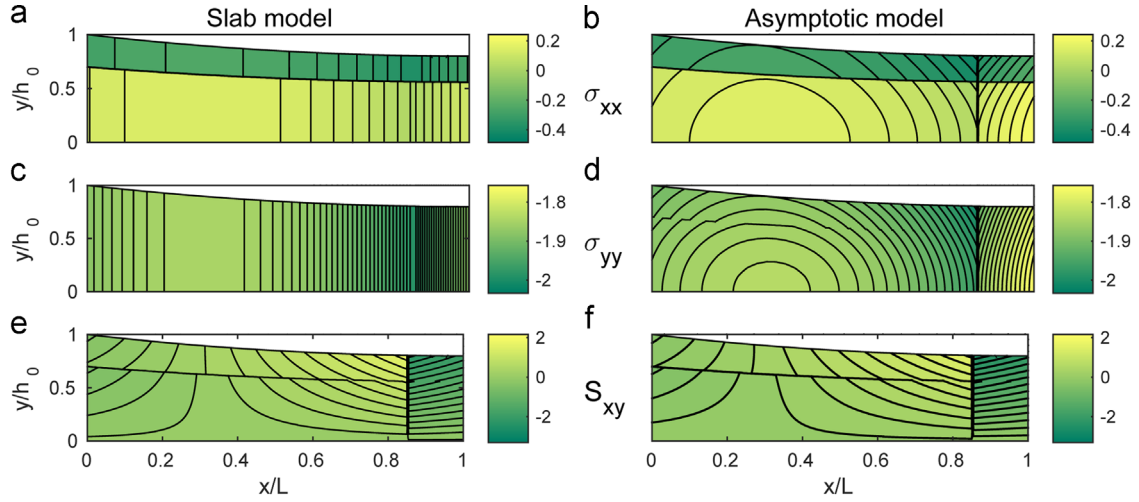

Fig. 7. Stresses in the roll gap for a moderate roller radius ($R = 0.1$ m, $\delta = 0.35$). The Cauchy stresses (a, b) σ_{xx}, (c, d) σ_{yy} and (e, f) S_{xy} are shown for the (a, c) slab model and (b, d) corrected asymptotic model.

balance. The second-order effect of the velocity shear is to increase the pressure (hence the magnitude of σ_{xx} and σ_{yy}) near the roller surface. The vertical velocity and shear stress distributions remain largely unaltered by the $O(\delta^2)$ correction.

For a larger roller radius ($R = 0.4$ m, $\delta = 0.18$), the velocity and stress distributions (illustrated in Figs. 8 and 9 respectively) differ. In this case, friction dominates in Eq. (26), and a classic 'friction hill' shape appears. The geometric term has only a very limited effect near the ends of the roll gap. Other than that the through-thickness variation of velocity and stress is slightly weaker than in the case of moderate roller radius. Nevertheless, the general effect of the $O(\delta^2)$ correction is essentially the same.

It is worth commenting on the apparent discontinuity in the shear stress at the interface between matrix and cladding material. This is a consequence of the assumption of continuous tangential stress, combined with the jump in σ_{xx} induced by the change in material yield stress. A similar discontinuity arises at second order in σ_{yy} for the same reason, although it is too small to be clearly visible in Fig. 9.

4.4. The effects of elasticity and smoothed friction

As seen in Section 4.1, neither the slab model nor the asymptotic model agrees quantitatively with the finite element simulations. This is in contrast to Montmitonnet [13], who successfully compared a slab model with finite element calculations of homogeneous rolling. However, Montmitonnet [13] used a purely plastic numerical solver. This suggests that the disagreement in the results presented here is mainly the consequence of the elastic–plastic flow rule used by Abaqus. This hypothesis seems to be supported in Fig. 10, which shows the stress components and von Mises stress evaluated at the roll surface. It is clear that the predictions of the analytical model are accurate for a large portion of the roll surface, but deviate significantly around the neutral point and at the entrance to the roll gap. Near the neutral point, numerical smoothing of the Coulomb friction condition leads to the rounded 'friction hill' obtained in the simulation. At the roll gap entrance, the simulated von Mises stress profile clearly indicates that the material is sub-yield over the first 20% of the roll gap, meaning that all of the strain is elastic, rather than plastic, in that section of the roll gap. In the bulk of the roll gap, the small difference between the theoretical von Mises yield stress and the simulated stress suggests that some small portion of the strain is elastic throughout the roll gap. Nevertheless, this seems not to influence the prediction of stress too strongly; there is good agreement between the predicted and simulated stresses for the remaining 80% of the roll gap.

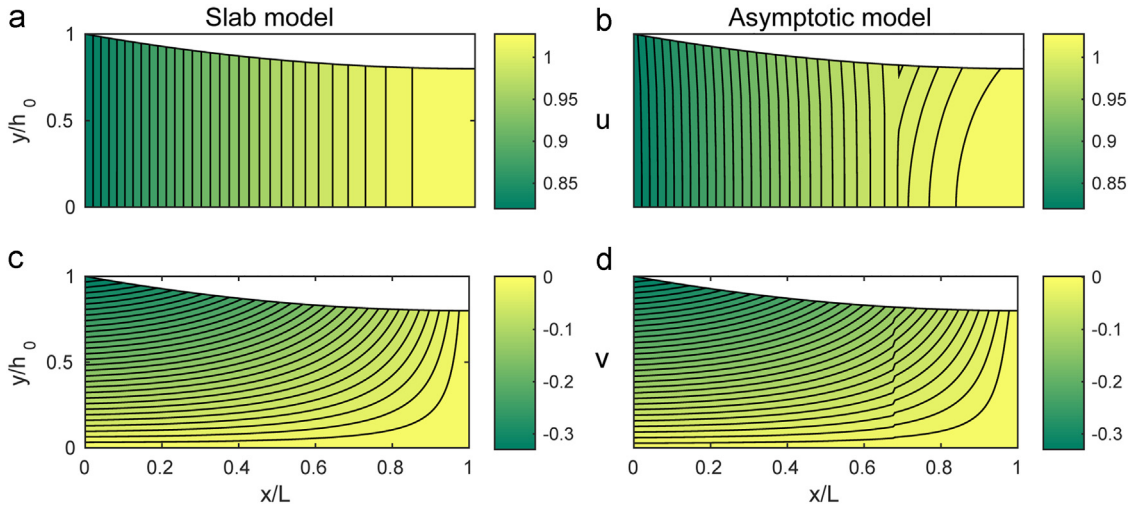

Fig. 8. Velocities in the roll gap for a larger roller radius ($R = 0.4$ m, $\delta = 0.18$). The (a, b) horizontal and (c, d) vertical velocities are shown for the (a, c) slab model and (b, d) corrected asymptotic model.

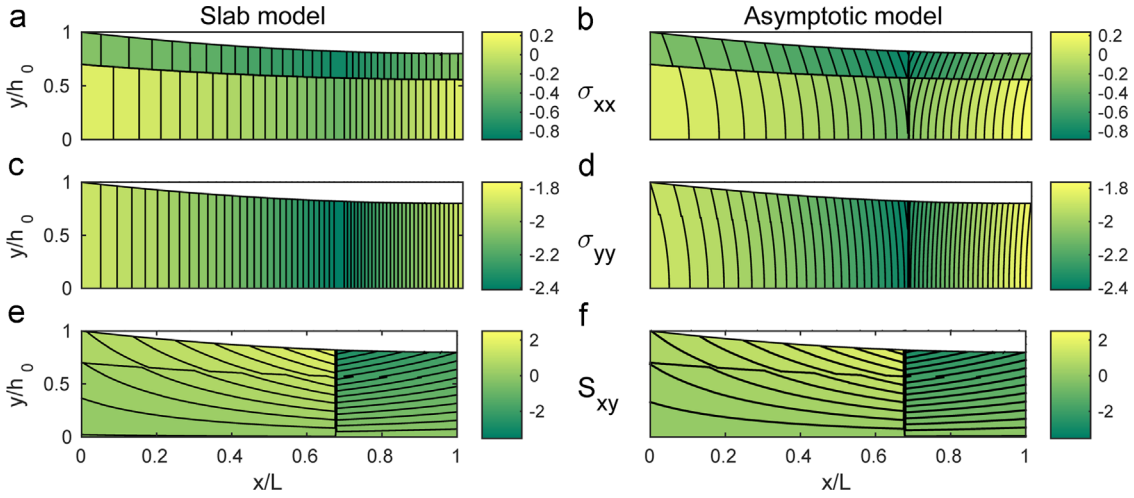

Fig. 9. Stresses in the roll gap for a larger roller radius ($R = 0.4$ m, $\delta = 0.18$). The Cauchy stresses (a, b) σ_{xx}, (c, d) σ_{yy} and (e, f) S_{xy} are shown (b, d, f) with and (a, c, e) without the asymptotic $O(\delta^2)$ correction derived in Section 2.3.

4.5. Solution times

An important benefit of using the asymptotic model presented in this paper over finite element simulations is a dramatic reduction in the time needed to calculate the stress and strain in the roll gap. A typical finite element simulation needed to generate one data point in Fig. 2, for example, required up to two hours CPU time on a standard desktop computer. By contrast, the solution to the asymptotic model was typically calculated in less than two seconds.

Approximately 60% of the CPU time required to calculate the asymptotic solution was needed to determine the leading-order solution. In particular, locating the neutral point was always the most time-consuming task. Adding the $O(\delta^2)$ correction contributed less than 40% to the computational cost.

5. Discussion

The results presented here show that the asymptotic model presented in this paper not only agrees well with the predictions of slab theory, somewhat validating its assumptions, but also provides additional information regarding the stress and velocity distributions throughout the rolled sheet. As expected, the slab result provides a good approximation to the stress distribution in the harder material when the yield stress ratio is particularly large or small.

However, some discrepancies were found between the analytical results and the results of finite element simulations. As suggested in Section 4.4, it seems to be the case that the elasticity required by Abaqus is the main reason for the difference. There have been previous attempts to incorporate elastic stresses in analytical models, particularly by considering a small elastic region at the start of a constriction in extrusion [10]. In that paper, the authors simply equate the elastic stress to the plastic stress at an arbitrary point near the entrance to the roll gap, creating an abrupt transition in material behaviour. While this seems to agree reasonably with their data, their data are relatively sparse and noisy. A more detailed treatment would be to consider elastic stresses alongside plastic stresses throughout the roll gap. This would add significant complication to the equations for sandwich rolling, and is perhaps better illustrated for traditional, homogeneous rolling. Such an analysis has not yet been presented in the literature.

Other future work could extend these results to allow for strain-hardening or work-hardening, temperature-dependent effects, or asymmetry between the pair of rolls (see [14] for a similar treatment of asymmetry in homogeneous rolling). Furthermore, one could attempt to remove the discontinuity in the region of the

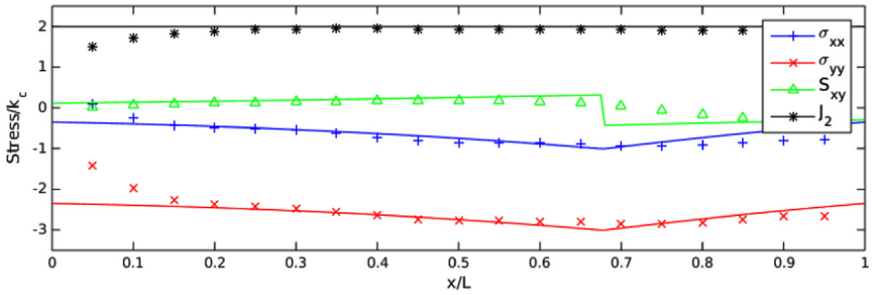

Fig. 10. Stress components and von Mises stress (J_2) plotted along the roll surface ($y = h(x)$) for the larger roller ($R = 0.4$ m, $\delta = 0.18$). Symbols show the simulated results, while curves show the predictions of the asymptotic model.

neutral point by considering alternative, more smooth friction models, such as the relative slip model used in [9]; or by performing a more sophisticated asymptotic analysis in the vicinity of the neutral point.

In summary, by relaxing the traditional assumption of stress homogeneity, a more detailed analytical model of the velocity and stress fields in sandwich rolling has been derived. The slab theory result of Tzou [7] was shown to be consistent with rolling at small aspect ratio, and the asymptotic model presented here is shown to give similar predictions for the roll force and torque across a range of material configurations, material properties, and rolling geometries. In particular, we showed the range of validity of this model under changes in roll radius, friction coefficient, and reduction. The additional predictions made by the asymptotic model regarding the stress and strain distributions obtained may be useful in predicting microstructural changes due to rolling throughout the thickness of the composite product, while the time required for numerical evaluation is much less than costly finite element simulations, making this model a good candidate for use in online process control.

Acknowledgements

The authors gratefully acknowledge funding under the EPSRC Grant RG68390. E.J.B. also acknowledges the support of a Royal Society University Research Fellowship and a College Lectureship at Gonville & Caius College, University of Cambridge. J.J.M. is supported by a Cambridge-Rutherford Memorial Scholarship from the Royal Society of New Zealand. The authors also thank Julian Allwood and Evros Loukaides for helpful discussions.

Appendix A. Supplementary data

Supplementary data associated with this paper can be found in the online version at http://dx.doi.org/10.1016/j.ijmecsci.2015.12.012.

References

[1] Afonja AA, Sansome DH. A theoretical analysis of the sandwich rolling process. Int J Mech Sci 1973;15:1–14.
[2] Arnold RR, Whitton PW. Stress and deformation studies for sandwich rolling hard metals. Proc Inst Mech Eng 1959;173:241–56.
[3] Tanaka E, Kukuda T, Suzuki Y, Nakamoto M. Cold clad rolling of copper-steel-copper. J Jpn Soc Technol Plast 1971;12:622–30.
[4] Shirota T, Dendo T. Some experiments on clad rolling by planetary mill in cold stage. J Jpn Soc Technol Plast 1983;24:53–8.
[5] Kiuchi M, Hwang YM, Shintani K. Analysis and experiment on sandwich sheet rolling. J Jpn Soc Technol Plast 1990;31:1445–50.
[6] Hwang YE, Hsu HH, Lee HJ. Analysis of sandwich sheet rolling by stream function method. Int J Mech Sci 1995;37:297–315.
[7] Tzou GY. Theoretical study on the cold sandwich sheet rolling considering Coulomb friction. J Mater Process Technol 2001;114:41–50.
[8] Domanti S, McElwain DLS. Two-dimensional plane strain rolling: an asymptotic approach to the estimation of inhomogeneous effects. Int J Mech Sci 1995;37:175–96.
[9] Cherukuri HP, Johnson RE, Smelser RE. A rate-dependent model for hot rolling. Int J Mech Sci 1997;39:705–27.
[10] Govindarajan RM, Aravas N. Asymptotic analysis of extrusion of porous metals. Int J Mech Sci 1991;33:505–27.
[11] Dassault Systèmes, Simulia Corp., Providence, RI, USA, Abaqus 6.12 Example Problems Manual.
[12] Karabin ME, Smelser RE. A quasi-three-dimensional analysis of the deformation processing of sheets with applications. Int J Mech Sci 1990;32:375–89.
[13] Montmitonnet P. Hot and cold strip rolling processes. Comput Methods Appl Mech Eng 2006;195:6604–25.
[14] Minton JJ, Cawthorn CJ, Brambley EJ. An asymptotic model of asymmetric rolling. Int J Mech Sci 2015, submitted for publication.